Gravitational waves from incomplete inflationary phase transitions

Joel Barir,* Michael Geller,† Chen Sun[®],‡ and Tomer Volansky[§] School of Physics and Astronomy, Tel Aviv University, Tel Aviv 69978, Israel

(Received 23 May 2022; revised 1 August 2023; accepted 16 November 2023; published 12 December 2023)

We study the observable implications of an incomplete first order phase transition during inflation. In such a phase transition, the nucleated bubbles do not percolate and instead are continuously produced until the onset of reheating. The process creates an inhomogeneity with a distinct power spectrum that depends on both the physics of the phase transition and the inflationary dynamics. Upon horizon reentry, this spectrum generates gravitational waves through nonlinear effects. This stochastic gravitational wave background is predicted to have unique signatures that may be detectable by future experiments spanning a wide frequency range. The discovery of such a gravitational wave signal would shed a light on the detailed dynamics of inflation.

DOI: 10.1103/PhysRevD.108.115016

I. INTRODUCTION

The detection of gravitational waves (GWs) by LIGO and VIRGO [1] has opened a new window into our universe. Upcoming and far future experiments are expected to cover a wide range of frequencies and also improve current sensitivities [2–12], making the future detection of a stochastic gravitational wave background possible. Intriguingly, the NANOGrav collaboration has reported some hints for the existence of a stochastic gravitational wave background at low frequencies of order 1 yr^{-1} [13], although it is not clear if the origin is cosmological. Since gravitational waves propagated freely through the universe even while it was opaque to light, a gravitational wave background of primordial origin, if it exists, can hold crucial information about the very early history of our universe.

Inflation is the leading paradigm for these first moments [14,15]. A period of rapid, exponential expansion explains why the observable universe is flat, homogeneous and isotropic to a very good accuracy. In the simplest scenario, the expansion can be driven by a single scalar field, called the inflaton. The initially small inhomogeneities of the universe originated in inflationary vacuum fluctuations, which grew to cosmological scales. These inhomogeneities are observed through the cosmic

Published by the American Physical Society under the terms of the Creative Commons Attribution 4.0 International license. Further distribution of this work must maintain attribution to the author(s) and the published article's title, journal citation, and DOI. Funded by SCOAP³.

microwave background (CMB), giving strong constraints on inflationary models [16-20]. For a review of inflation, see [21].

GWs provide a promising tool to further explore the inflationary epoch. Although nothing is known about the pre-inflationary epoch, it is commonly assumed that the universe has been in a high-energy state. During inflation, the universe has rapidly cooled and it is natural to expect the system to be away from its global minimum, which may be eventually reached through one or more phase transitions (PTs). It is conceivable that some of these PTs are first order and proceed through bubble nucleation. Fast enough first order PTs proceed through a percolation stage which produce (possibly observable) GWs [22-25] (for GWs from PTs after inflation, see, e.g., [26–39]). Another possibility, however, which is at the focus of this paper, is slow PTs, which do not complete during inflation. In that case, bubbles nucleate too far from each other and never go through the percolation stage, due to the shrinking Hubble sphere. One may therefore wonder whether a GW signal still forms and if so, how would it be distinguished from the previously studied scenarios?.

As we show below, while bubbles do not collide and percolate, their presence serves as a new source of inhomogeneities on small length scales. As a consequence of the PT remaining incomplete during inflation, the bubbles are produced continuously, resulting in a broad and flat inhomogeneity spectrum, spanning across a large range of modes. After inflation, once those modes enter the horizon, the inhomogeneities induce GWs through secondary effects [41–46] with a similarly broad and rather unique spectrum which could be measured by multiple

joelbari@mail.tau.ac.il

micgeller@tauex.tau.ac.il

chensun@mail.tau.ac.il

^{\$}tomerv@post.tau.ac.il

¹A different example for a model featuring an incomplete PT can be found in [40].

upcoming and future experiments. The spectrum depends not only on the sector which goes through the PT but also on the details of inflation.

To demonstrate the above, we study a simplified single-field model which captures the relevant features of various PTs, including the well-known Coleman-de Luccia (CdL) bubble nucleation [47] and the Hawking-Moss (HM) instanton [48]. We then calculate the expected anisotropies and resulting GW background, concluding that a new and promising signal may appear in future GW observatories, shedding light on hidden sectors as well as on the physics of inflation.

II. INFLATION AND PHASE TRANSITIONS

A first order PT in the early universe takes place via bubble nucleation. The bubbles may or may not collide depending on the competition between their expansion and nucleation rates with the expansion rate of the universe. In this sense, such phase transitions exhibit two distinct regimes. The phenomenology of PTs with bubble collisions has been thoroughly studied [22–39], and here we focus on the signatures of PTs where the bubbles cannot meet.

During inflation, any slow enough first order PT does not complete [49,50]. Schematically, if the bubble nucleation rate per unit volume is smaller than the Hubble expansion rate, i.e.,

$$\Gamma/V \lesssim H^4$$
, (1)

the mean distance between two neighboring bubbles is larger than the cosmological horizon (which shrinks in comoving coordinates). Hence bubbles cannot meet and percolate, leaving most of space in the false vacuum and the transition incomplete for as long as the universe inflates. While signals, such as GWs, are typically known to be produced during the percolation period, in this paper we show that stochastic GW signals are also predicted in slow PTs that cannot percolate during inflation, and the resulting signal records the entire duration of the PT.

To be concrete, consider first the CdL tunneling process [47] which describes the quantum process of vacuum tunneling in a gravitational background, and the rate of which is calculated with the instanton method based on the saddle-point approximation. In the semiclassical calculation, the bubbles are produced at rest with their radius equal to the critical radius—the minimal radius for an expanding bubble. Once formed, such bubbles expand classically, quickly approaching the speed of light. As soon as the physical radius of the bubble becomes larger than the Hubble radius, H^{-1} , the surface velocity becomes negligible and the Hubble drift dominates the bubble evolution. At this point the bubble is "frozen," i.e. it does not expand with respect to the comoving frame. As a consequence, a single bubble can never overtake the entire

universe and for low enough nucleation rate, too few bubbles can form to complete the PT.

The Hubble radius represents the region contained inside a cosmological horizon created by the expanding universe. Therefore, in order to maintain causality, a CdL bubble must form with a smaller radius and if the critical bubble radius is larger than H^{-1} , the CdL instanton does not exist. Instead, tunneling is still possible through the HM solution [48]. In the HM case, an entire Hubble patch tunnels simultaneously to the top of the potential barrier. This phenomenon is best understood through the formalism of stochastic inflation [51] where the inflationary horizon gives rise to a temperature, analogous to the Hawking temperature of a black hole. The thermal fluctuations then allow a trapped scalar field to diffuse, eventually reaching the top of a potential barrier. Once the barrier is crossed, the field may classically roll to the true minimum. As with the CdL PT, here too the Hubble-size bubble remains frozen and a slow nucleation rate implies that the PT is never complete. However, as opposed to the CdL case, the stochastic formalism shows that the HM instanton calculation only holds in the limit of a very slow transition [51,52], and thus by construction can only describe an incomplete PT during inflation.

III. A MODEL

The necessary details needed to study an incomplete PT can be described by a simple toy model. The PT is driven by the field χ , acting as a spectator during inflation. The inflationary dynamics are dominated by the inflaton ϕ , for which we assume the slow-roll conditions to hold, but whose detailed potential we otherwise remain agnostic to. While interactions between χ and ϕ may exist, their presence do not significantly affect our conclusions and we ignore them here. The potential is thus

$$V = V_{\rm PT}(\chi) + V_{\rm inf}(\phi), \tag{2}$$

where,

$$V_{\rm PT}(\chi) \ll V_{\rm inf}(\phi)$$
. (3)

The PT potential, $V_{\rm PT}(\chi)$, is illustrated in Fig. 1. In the case of CdL tunneling, we take χ to be initially on the left side of the potential and away from the false vacuum, classically slow-rolling down. In the case of HM transition, an initial slow-roll is not necessary, and χ may initially be set at the local minimum. In this scenario, the phase transition begins after relaxation of the probability distribution for χ . As an example, we discuss the latter possibility within the context of a concrete model in Appendix A. In either case, we define t_0 as the moment when bubble production starts, which is determined by either the duration of classical rolling, or the relaxation time from stochastic inflation. To evade CMB constraints [16–20]

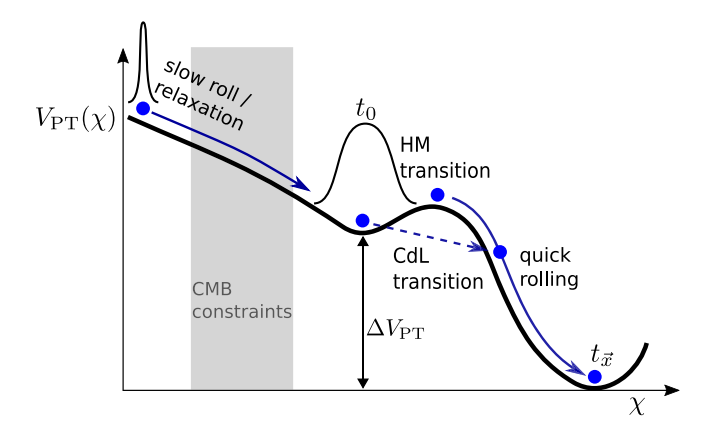


FIG. 1. Evolution of the spectator field, χ , that drives the phase transition. A slow-rolling or relaxation phase allows for the creation of the almost scale-invariant power spectrum observed at large scales in the CMB. The times probed by the CMB are illustrated with the gray-colored region. At some later time t_0 , the field gets stuck in a local minimum of the potential, or in the case of HM transition, relaxes into a stable probability distribution around it. The field may escape this local minimum before the end of inflation through either Coleman-de Luccia (CdL) or Hawking-Moss (HM) tunneling, creating inhomogeneities in the energy density. Under the assumption of low bubble nucleation rate, this phase transition is never completed during inflation. We assume $V(\chi) \ll V(\phi)$ where ϕ is the inflaton field, for the entire duration of inflation.

we assume t_0 is sufficiently late in the inflationary epoch, so that bubble nucleation takes place only after the CMB modes had exited the horizon. Once a bubble is produced, χ inside it can roll to the global minimum where $V_{\rm PT}=0$, making it a true vacuum bubble. For simplicity, we assume this classical rolling after barrier crossing to be instantaneous.

The bubble nucleation rate during the PT is directly dictated by the potential parameters. We thus choose $V_{\rm PT}$ such that Eq. (1) is fulfilled, ensuring a slow PT and implying that the physical volume of space where χ is "stuck" in the unstable minimum increases with time. Once the inflaton decays, regions of false vacuum may dominate the energy density and lead to an unwanted eternal inflation within our Hubble patch, driven by χ . To evade such a catastrophe, one may either assume that the reheating temperature is larger than the energy density in the false vacuum and its effect drives to destabilize it, or even simpler, that the nucleation rate is larger than the value of Hubble in the false vacuum so that rapid nucleation and percolation becomes possible after the inflaton decays.² With this, the PT suddenly and instantaneously completes everywhere and inflation truly ends at least within our visible universe.

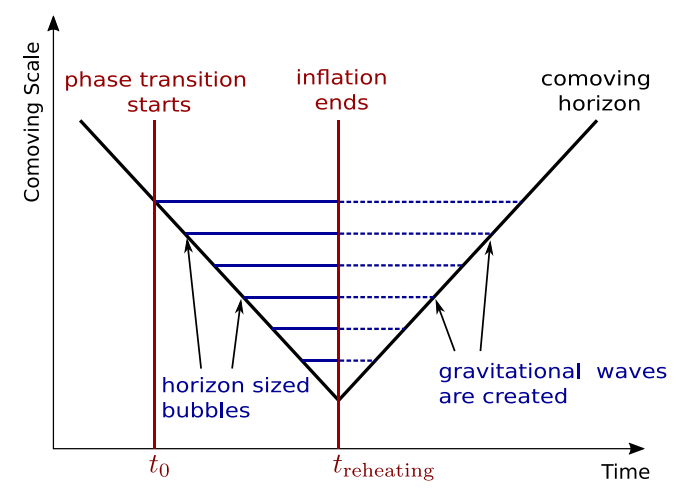


FIG. 2. The process of bubble formation and GW production on comoving scales. Bubbles are formed equally at all times from the beginning of the phase transition and until the end of inflation. These bubbles quickly grow to horizon size and freeze in the case of Coleman-de Luccia tunneling, or form frozen at horizon size through Hawking-Moss tunneling. In either case, when inflation ends, the transition completes due to the reduced expansion rate or increased temperature. The inhomogeneity introduced by the bubbles remains, generating GWs upon horizon re-entry.

The process of horizon exit and re-entry is illustrated in Fig. 2. The bubbles are either created small and rapidly expand to horizon size, as in the case of CdL, or created exactly at horizon size, as in the case of HM. Either way, once at the horizon, the comoving radius is completely frozen. After the end of inflation, the phase transition completes everywhere but the imprint on the curvature power spectrum remains. Upon horizon reentry, the inhomogeneities produce GWs from secondary effects. Independent of the fine details of the model, the dynamics are governed by merely three parameters: the tunneling rate per unit volume Γ/V , the vacuum energy difference $\Delta V_{\rm PT}$ between the false and true vacuum, and the time t_0 at which the transition commences (shortly after γ reaches the false vacuum). With this simplified description we now turn to calculate the GW spectrum produced by such inflationary incomplete PTs and arrive at predictions for future experiments. In Appendix A, we provide a concrete example for a potential of the form described here, and show how the relevant results depend on the underlying couplings.

IV. SCALAR CURVATURE SPECTRUM

We now move to calculate the scalar spectrum. To this end, we first find the energy-momentum tensor $T_{\mu\nu}$, neglecting the energy density in the bubble wall. This is justified because the ratio of energy in the interior volume over the wall energy scales as a (the metric scale factor), and grows as the universe rapidly expands. Given the above, we omit the spatial derivatives of χ and ϕ , which are

²We will ignore the GW from this final stage of the PT, as these occur not far from the reheating time, and the frequency range is likely beyond any near-future experiment.

localized in the bubble walls, and write the energy density and pressure after the PT starts, at $t \ge t_0$,

$$\rho, p = \frac{1}{2}\dot{\phi}^2 \pm V_{\text{inf}}(\phi(t)) \pm \left[1 - \theta(t - t_{\vec{x}})\right] \Delta V_{\text{PT}}.$$
 (4)

Here $t_{\vec{x}}$ is the time when the transition occurred at point \vec{x} , and θ is the Heaviside step function. Using a step function is justified under the assumption of a rapid roll to the true vacuum after χ tunnels out of the false minimum. This rapid roll will not necessarily be immediate after tunneling: Any delay between tunneling and rolling to the true vacuum can be regarded as a shift in t_0 . Furthermore, the kinetic energy stored in χ around the true minimum is quickly dissipated and is therefore neglected. All other components of the energy-momentum tensor can be neglected.

The main effect of the PT on the curvature spectrum is through the change in the Hubble constant due to the shift in the vacuum energy. We use the linearized Einstein equations in Newtonian gauge to calculate this induced curvature perturbation to first order. To this end, we need to find the inhomogeneous part of $T_{\mu\nu}$:

$$\rho(t, \vec{x}) = \bar{\rho}(t) + \delta \rho(t, \vec{x}), \qquad \delta \rho \ll \rho, \tag{5}$$

and similarly for p. The homogeneous background is taken to be

$$\bar{\rho}, \bar{p} = \frac{1}{2}\dot{\phi}^2 \pm V_{\rm inf}(\phi(t)) \pm \left[1 - \theta(t - \langle t_{\vec{x}} \rangle)\right] \Delta V_{\rm PT},$$
 (6)

while the perturbations are given by

$$\delta\rho(t,\vec{x}) = \Delta V_{\rm PT} \left[\theta(t - \langle t_{\vec{x}} \rangle) - \theta(t - t_{\vec{x}}) \right], \tag{7}$$

and $\delta p = -\delta \rho$. The (scalar) perturbed metric in Newtonian gauge (for a review see, e.g., [21]) is,

$$ds^{2} = -(1 + 2\Phi)dt^{2} + a^{2}(t)(1 - 2\Psi)(dx^{2} + dy^{2} + dz^{2}),$$
(8)

and the gauge invariant comoving curvature perturbation is defined as

$$\mathcal{R} = \Psi - \frac{H}{\bar{\rho} + \bar{p}} \delta q, \tag{9}$$

where δq is the scalar momentum perturbation. When specifying the energy momentum tensor in Eqs. (6) and (7), we have neglected the wall energy, which is equivalent to setting $\delta q = 0$ and $\mathcal{R} = \Psi$.

The only Einstein equation we will need for calculating $\ensuremath{\mathcal{R}}$ is

$$\dot{\mathcal{R}} + H\Phi = 0. \tag{10}$$

Using the continuity equation

$$\delta p + (\bar{\rho} + \bar{p})\Phi = 0, \tag{11}$$

we extract Φ and plug the result into Eq. (10),

$$\dot{\mathcal{R}} = H \frac{\delta p}{\bar{\rho} + \bar{p}} = -H \frac{\delta \rho}{\dot{\phi}^2}.$$
 (12)

Equation (7) shows that \mathcal{R} is constant for $t < t_1 = \min(t_{\vec{x}}, \langle t_{\vec{x}} \rangle)$ and for $t > t_2 = \max(t_{\vec{x}}, \langle t_{\vec{x}} \rangle)$. For simplicity, and using the slow-roll approximation, we take $\dot{\phi}$ and H to be constant and assume an initial flat background. We will later relax these assumptions in order to demonstrate the sensitivity of the predicted spectrum to the inflationary dynamics. The integrated Eq. (12) then gives

$$\mathcal{R}(\vec{x}) = -\frac{H\Delta V_{\text{PT}}}{\dot{\phi}^2} \left(t_{\vec{x}} - \langle t_{\vec{x}} \rangle \right) \equiv -\frac{H\Delta V_{\text{PT}}}{\dot{\phi}^2} \delta t_{\vec{x}}. \tag{13}$$

We move to calculate the scalar power spectrum $\mathcal{P}_{\mathcal{R}}(k)$, defined by

$$\langle \mathcal{R}_{\vec{k}} \mathcal{R}_{\vec{k}'} \rangle = \delta(\vec{k} + \vec{k}') \frac{2\pi^2}{k^3} \mathcal{P}_{\mathcal{R}}(k).$$
 (14)

Equation (13) implies that one has to calculate the correlation between the tunneling times at different points in space, $\langle \delta t_{\vec{x}} \delta t_{\vec{x}} \rangle$. The details of this calculation are given in Appendix B, where we assume spherical bubbles and a constant tunneling rate Γ/V . The calculation further assumes that bubbles nucleate frozen at horizon size, a valid assumption in the HM case, and a reasonable approximation in the CdL case.

The scalar spectrum is shown in Fig. 3 for three different choices of the relevant parameters. The PT commences at t_0 and carries on until the end of inflation at $t_{\text{reheating}}$, continuously producing bubbles. The effect on the primordial power spectrum therefore spans the range of momentum modes that exit the horizon at this period of time, i.e., from $k_0 \equiv Ha(t_0)$ to $k_{\rm re} \equiv Ha(t_{\rm reheating})$. Since bubbles are created at a fixed rate in a universe with a shrinking co-moving Hubble sphere, the spectrum is expected to be approximately flat (varying only logarithmically). For concreteness, throughout this work we fix $k_{\rm re} = 4 \times 10^{22} \ {\rm Mpc^{-1}}$. Under our assumptions above of inflation with fixed slow-roll parameters, the shape and position of the peak are determined by the two k's, while the amplitude further depends linearly on the dimensionless parameter $\gamma_{\rm PT} \equiv \frac{1}{H^4} \frac{\Gamma}{V} \left(\frac{\Delta V_{\rm PT}}{\dot{\rho}^2}\right)^2$ [see Eqs. (13) and (14) as well as Appendix B for details]. We find that the maximal value of the power spectrum, $\mathcal{P}_{\mathcal{R}}$ only weakly depends on k_{0} and is roughly $\mathcal{P}_{\mathcal{R},\text{max}}/\gamma_{\text{PT}} \approx \mathcal{O}(10^3)$. With the scalar spectrum calculated, we move on in Sec. V to calculate the GW spectrum it generates in the radiation-dominated era.

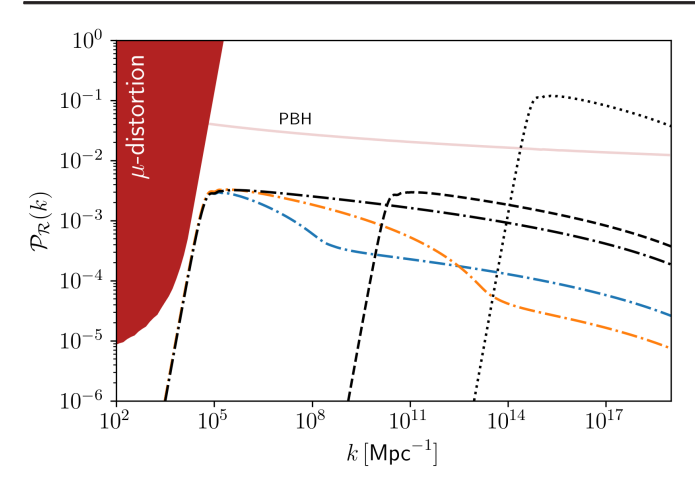


FIG. 3. The scalar spectrum $\mathcal{P}_{\mathcal{R}}$, shown for different choices of the parameters. The dimensionless parameter $\gamma_{\rm PT} \equiv \frac{1}{H^4} \frac{\Gamma}{V} (\frac{\Delta V_{\rm PT}}{\dot{a}^2})^2$, which is assumed to be constant, linearly controls the amplitude. The momentum scale of the horizon at the beginning of the phase transition, $k_0 \equiv Ha(t_0)$, acts as a minimal scale, below which the spectrum is strongly suppressed. The scale of reheating $k_{\rm re} \equiv Ha(t_{\rm reheating})$ was fixed at $4 \times 10^{22} \,{\rm Mpc^{-1}}$. The black dash-dotted, dashed, and dotted lines correspond to the parameter choices $k_0 = 2 \times 10^4$, 8×10^9 , 2×10^{14} Mpc⁻¹ and $\gamma_{PT} = 5 \times 10^{-7}$, 10⁻⁶, 10⁻⁴, respectively. The blue and orange dashed-dotted lines show the spectrum for an alternative scenario where the value of $\frac{H}{b^2}$ changes by a factor of 1/10 at time t_{drop} . We define $k_{\rm drop} \equiv Ha(t_{\rm drop})$ and take its value to be $k_{\rm drop} = 10^8, 10^{13}~{\rm Mpc^{-1}}$ for the blue and orange lines respectively. We further choose $k_0=2\times 10^4$ and $\gamma_{\rm PT}=7\times 10^{-6}, 2\times 10^{-6}$ to ensure that the peaks align, thereby demonstrating the effect of the drop in $\frac{H}{\lambda^2}$ on the spectral shape. The colored lines demonstrate how the spectral shape probes the dynamics of inflation over the duration of the phase transition. The red region is excluded by existing bounds on CMB spectral distortions [53]. The pale red line represents existing bounds from constraints on primordial black holes, taken from [19]. This line is not accurate, because known bounds assume Gaussianity.

We emphasize that the power spectrum is sensitive not only to the spectator field which drives the PT, but also to the inflationary dynamics themselves, and its shape records the entire inflationary history from the beginning of the PT to the onset of reheating. Consequently, a measurement of the spectral shape can reveal detailed information about the dynamics of inflation. So far, we have assumed that the slow-roll parameter and scale of inflation are constant [see Eqs. (12) and (13)]. Relaxing this assumption strongly affects the spectrum as is demonstrated by the blue and orange dashed-dotted lines in Fig. 3, which assume a sudden change in the value of $\frac{H}{\phi^2}$ occurring at time $t_{\rm drop}$. For a detailed derivation of $\mathcal{R}(\vec{x})$ in this case, we refer the reader to Appendix C.

Figure 3 further shows constraints from the overclosure due to primordial black hole (PBH) abundance (red line), and distortions to the CMB black-body spectrum (red region). We note that the PBH constraint, taken from [19], assumes a Gaussian $\mathcal{P}_{\mathcal{R}}$. The line shown in Fig 3 is therefore only a rough estimation. To derive the exact bound of PBH abundance on the spectrum, a model-specific calculation, which considers the non-Gaussian statistics of the phase transition, is required and goes beyond the scope of this paper.

Due to the highly non-Gaussian nature of the spectrum, it may be possible to search for the non-Gaussianities of the primordial perturbations directly in the CMB. This is relevant for the case where the phase transition starts earlier at inflation, where the CMB is sensitive to much lower amplitudes. In this scenario, there will be no signals for GW detectors. We leave the analysis of the CMB phenomenology for future work.

V. GRAVITATIONAL WAVE SPECTRUM

After horizon reentry, the curvature perturbations produce GWs through second order effects. A general prescription for calculating GWs induced during the radiation dominated era is derived in [45,46], where the inhomogeneity was assumed to be Gaussian. This allows the use of Wick's theorem to reduce the four-point correlation functions of \mathcal{R} into products of two-point correlations, i.e. the power spectrum $\mathcal{P}_{\mathcal{R}}$. Although the phase transition spectrum is very far from Gaussianity, we have found that the result [45,46] still applies, because the "connected" part of the four-point correlation function does not induce GWs. This point is further explained and proven in Appendix D. In the following we briefly review the relevant result of [45,46], before applying it to the spectrum derived in the previous section.

The GW energy density parameter is given by

$$\frac{d\Omega_{\rm GW}}{d\log k}(\eta, k) \equiv \frac{1}{\rho_{\rm tot}} \frac{d\rho_{\rm GW}}{d\log k} = \frac{1}{24} \left(\frac{k}{a(\eta)H(\eta)}\right)^2 \overline{\mathcal{P}_h(\eta, k)},\tag{15}$$

where η is the conformal time and $\overline{\mathcal{P}_h(\eta,k)}$ is the time averaged tensor spectrum, given by

$$\overline{\mathcal{P}_{h}(\eta, k)} = 4 \int_{0}^{\infty} dv \int_{|1-v|}^{1+v} du \left(\frac{4v^{2} - (1+v^{2} - u^{2})^{2}}{4vu}\right)^{2} \times \overline{\tilde{I}^{2}(v, u, k\eta)} \mathcal{P}_{\mathcal{R}}(kv) \mathcal{P}_{\mathcal{R}}(ku). \tag{16}$$

Here the quantity $\overline{\tilde{I}^2(v,u,k\eta)}$ is defined in Eq. (D4).

 $d\Omega_{\rm GW}/d\log k$ approaches a constant value during radiation domination because the GWs redshift like radiation. The density during radiation domination can thus be related to the density today through

$$\frac{d\Omega_{\text{GW}}(\eta_0, k)}{d\log k} = \Omega_r(\eta_0) \frac{d\Omega_{\text{GW}}(\eta_c, k)}{d\log k}, \quad (17)$$

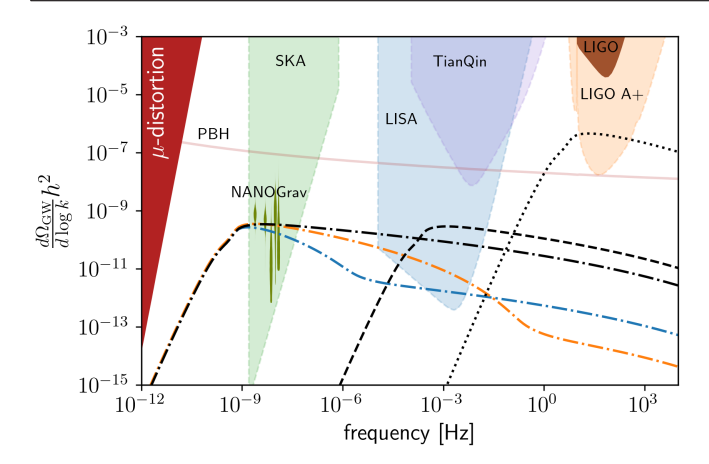


FIG. 4. The GW energy density induced by the scalar spectra shown in Fig. 3. For the model parameters, see the caption to Fig. 3. Current constraints and future detector sensitivity regions are shown with solid, and semitransparent colored regions respectively. The detector sensitivity curves for SKA [54], LISA [3,55], TianQin [4], LIGO [2], and LIGO A+, are taken from [56]. The green violin plots represent the free-spectrum fit to the NANOGrav data [13,57]. The red region and pale red line are CMB distortion and primordial black hole constraints derived from those in Fig. 3.

where $d\Omega_{\rm GW}(\eta_c,k)/d\log k$ is the constant value reached during the radiation dominated era, and $\Omega_r(\eta_0) \approx 10^{-4}$ is the energy fraction of radiation today.

Integrating Eq. (16) numerically, we obtain the GW spectrum shown in Fig. 4 for the parameters discussed in Sec. IV. Since the scalar spectrum is almost scale-invariant over a wide range of momenta, the induced abundance of GWs can be approximated by the analytical result given in [45] for a scale invariant case, $d\Omega_{\rm GW}(\eta_c,k)/d\log k \simeq 0.8 \mathcal{P}_{\mathcal{R}}^2$. Applying this approximation along with Eq. (17), we find that much like the power spectrum, the peak of the GW energy density today can be estimated directly from the model parameters,

$$\left. \frac{d\Omega_{\rm GW}(\eta_0, k)}{d \log k} \right|_{\rm peak} \simeq \mathcal{O}(100) \gamma_{\rm PT}^2. \tag{18}$$

In addition to the predicted lines, Fig. 4 shows the corresponding constraints from Fig. 3, as well as constraints from LIGO [2] and expected sensitivity from various future GW detectors. See caption for details.

ACKNOWLEDGMENTS

We thank Nadav Outmezguine for useful discussions. The work of T. V. is supported by the Israel Science Foundation (Grant No. 1862/21), by the Binational Science Foundation (Grant No. 2020220) and by the European Research Council (ERC) under the EU Horizon 2020 Programme (ERC-CoG-2015—Proposal n. 682676 LDMThExp). M. G. is supported in part by Israel

Science Foundation under Grant No. 1302/19. M. G. is also supported in part by the US-Israeli BSF grant No. 2018236.

APPENDIX A: A MODEL

In this section, we provide a concrete example for the model potential described in Sec. III and Fig. 1. The example will be shown to satisfy the assumptions made within the text, which validates the results in our work, and in particular, the predicted gravitational wave signal.

We consider a simple renormalizable potential,

$$V_{\text{PT}}(\chi) = \frac{m_{\chi}^2}{2} \chi^2 - \frac{m_{\chi} \lambda_3}{3} \chi^3 + \frac{\lambda_4}{4} \chi^4,$$
 (A1)

and assume the couplings are positive, $0 < \lambda_4, \lambda_3$, corresponding to a potential barrier between the false vacuum at the origin and the deeper global minimum, see Fig. 5. The figure also shows how a finite reheating temperature can destabilize the false vacuum, as we discuss below. The mass m_{γ} is taken to be smaller than the Hubble scale, $m_{\gamma} < H$, and the resulting tunneling from the false vacuum in this example is via the Hawking-Moss instanton. The gravitational wave signal is controlled by both the tunneling rate and the energy difference ΔV_{PT} . To get a sizable gravitational wave signal, the height of the potential barrier has to be small compared to $\Delta V_{\rm PT},$ which translates to $\lambda_4 \ll \lambda_3^2$. We note that such a choice is stable under radiative corrections.³ One could also consider a different setting where higher dimensional operators stabilize the true minimum (rather than $\lambda_4 \chi^4$), providing a natural explanation for the smallness of the coupling. We focus the analysis on the potential given in Eq. (A1) for simplicity.

We now discuss the initial condition of χ that will result in the dynamics described in this work. It is impossible to know the correct initial conditions of the universe, so we will limit ourselves to analyzing whether the initial conditions necessary here are reasonable and require no finetuning. We assume that at some point during inflation, but significantly before the CMB modes exit the horizon, χ is at the false vacuum. This would be the case if the original initial conditions are sufficiently broad, so that some Hubble patches end up at the false vacuum. Even if most of the patches go down to the true vacuum, almost immediately thereafter, the false vacuum patches come to dominate the volume of the universe due to its higher Hubble constant and therefore exponentially faster expansion rate. This argument can be complicated if inflation is eternal—in which case it is muddled by the "measure problem." We do not address this issue here, and we will only assume that this initial condition is reasonable. Since the initial condition is homogeneous over our

 $^{^3}$ It is straightforward to check that the barrier height and $\Delta V_{\rm PT}$ do not change when considering the full 1-loop Coleman Weinberg potential, even though the fourth derivative around the false vacuum scales as λ_3^4 .

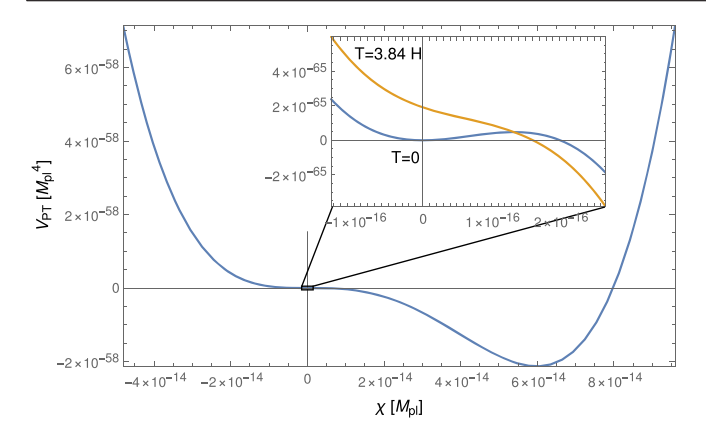


FIG. 5. The potential given by Eq. (A1), with $m_{\chi}=0.4H$, $\lambda_3=0.3$, $\lambda_4=2\times10^{-4}$, and $H=10^{-16}M_{\rm pl}$. The orange line shows the effective potential at a finite reheating temperature of T=3.84H, see the reheating model in Appendix A 2. This line shows the false vacuum is unstable at that reheating temperature, making the phase transition complete at reheating.

observable universe, this amounts to a δ -function distribution centered at some random point (of order $H/2\pi$) in the vicinity of the false vacuum. As the field continues to fluctuate, its distribution function broadens until it has finite support around the top of the potential barrier, allowing for the HM PT to take place. In accordance, bubble production will not commence immediately, but only after a relaxation time corresponding to the time it takes the distribution function to sufficiently broaden, providing the necessary delay for evading CMB constraints. Using the analytical solution of the Fokker-Planck equation for a quadratic potential [58], we can estimate the relaxation time as $t_{\rm rel} \approx \frac{3H}{m_{\rm v}^2}$. For the value used in the plots of this section, $m_{\gamma} = 0.4H$, the relaxation time is therefore of order $\sim 20H^{-1}$. Before relaxation completes, the tunneling rate is exponentially suppressed.

The peak of the potential barrier is located at $\chi_{\rm peak} \approx m_\chi/\lambda_3$, where the cubic term becomes comparable in size to the mass term. The peak value is thus given by

$$V_{\text{PT}}(\chi_{\text{peak}}) = \frac{m_{\chi}^4}{2\lambda_3^2} \left(\frac{1}{3} + \frac{\lambda_4}{2\lambda_3^2}\right) \simeq \frac{m_{\chi}^4}{6\lambda_3^2},$$
 (A2)

where for the last step we assumed $\lambda_4 \lesssim \lambda_3^2$. Similarly, the global minimum corresponds to $\chi_{\min} \approx m_{\chi} \lambda_3 / \lambda_4$, where the quartic term becomes important. The difference between the two local minima of the potential is therefore

$$\Delta V_{\rm PT} \simeq V_{\rm PT}(0) - V_{\rm PT}(\chi_{\rm min})$$

$$= m_{\chi}^4 \left(\frac{\lambda_3^4}{12\lambda_4^3} - \frac{\lambda_3^2}{2\lambda_4^2} \right) \simeq \frac{m_{\chi}^4 \lambda_3^4}{12\lambda_4^3}. \tag{A3}$$

Comparison of Eq. (A2) with Eq. (A3) shows that the barrier height is small compared to $\Delta V_{\rm PT}$ for $\lambda_4 \lesssim \lambda_3^2$,

as mentioned above. $\Delta V_{\rm PT}$ is further assumed to be small in comparison to the total energy density of the universe during inflation. To find the relative contribution of $V_{\rm PT}$ to the energy density, we divide Eq. (A3) by $V_{\rm tot} = 3 M_{\rm pl}^2 H^2$, yielding

$$\frac{\Delta V_{\rm PT}}{V_{\rm tot}} \approx 3 \times 10^{-2} \frac{m_{\chi}^4}{M_{\rm pl}^4 H^2} \frac{\lambda_3^4}{\lambda_4^3}.$$
 (A4)

This quantity is indeed small for $m_{\chi} \lesssim \frac{\lambda_3 \sqrt{M_{\rm pl} H}}{\lambda_4^{3/4}}$. The inequality is naturally satisfied in a large part of the relevant parameter range.

The χ field tunnels through the Hawking-Moss instanton and we have approximated the subsequent evolution of χ by a step function. The classical dynamics of χ are governed by the equation of motion

$$\ddot{\chi} + 3H\dot{\chi} + V'_{PT}(\chi) = 0. \tag{A5}$$

With the initial condition set past the potential barrier, the field rolls toward the true minimum and then oscillates around it. This is illustrated by a numerical solution in Fig. 6, where the initial condition was set beyond the potential barrier, at a point where the classical drift becomes dominant over quantum fluctuations. Rolling to the true vacuum does not necessarily occur immediately once the barrier is crossed— χ may remain in the vicinity of the false vacuum for numerous Hubble times after tunneling over the barrier. Our assumptions only require that most of the distance is covered over a short time, allowing the transition to be regarded as a step function. Any delay caused by classical rolling after a tunneling event is equivalent to a shift in the initial time of the transition t_0 .

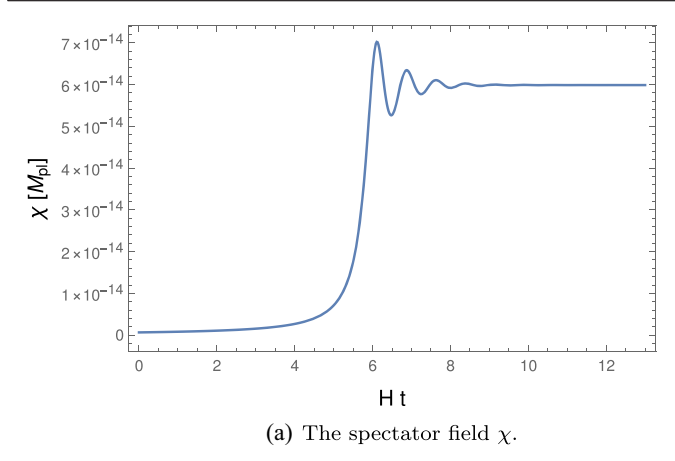
The solution is well approximated by a step function if rolling covers the distance to the true minimum in no more than few Hubble times, and the subsequent oscillations decay similarly quickly. The time the field takes to traverse to the true minimum can be estimated using the maximal velocity the field achieves over the rolling phase. Under the slow-roll approximation, the velocity can be written as $\dot{\chi} \approx -\frac{V'(\chi)}{3H}$, and the peak velocity is

$$\dot{\chi}_{\text{peak}} \simeq -\frac{V'\left(\frac{2\lambda_3 m_{\chi}}{3\lambda_4}\right)}{3H} \simeq \frac{4\lambda_3^3 m_{\chi}^3}{81\lambda_4^2 H}.$$
 (A6)

With this velocity, the duration of travelling to the true minimum at χ_{\min} is $\chi_{\min}/\dot{\chi}_{\text{peak}}$. Requiring this timescale to be no more than one Hubble time H^{-1} yields the condition

$$\frac{m_{\chi}^2}{H^2} \gtrsim \frac{81\lambda_4}{4\lambda_3^2}.\tag{A7}$$

Having found the condition for the rolling velocity, it remains to check the effect of subsequent oscillations.



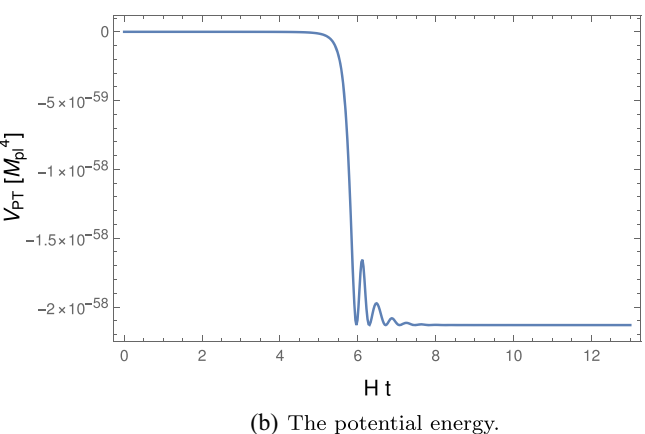


FIG. 6. Classical solution for χ after tunneling through the barrier shown in Fig. 5. This solution is assumed to be a step function throughout this work. The numerical solution here demonstrates the assumption is justified, as the energy quickly changes between two values in few Hubble times. The changes in energy density over time away from the "step" are smaller than the difference between the two values by orders of magnitude. The initial conditions were set to $\chi(t=0)=5m_\chi/\lambda_3$, outside the local potential well, and $\dot{\chi}(t=0)=-V'(\chi)/(3H)$, the slow-roll velocity.

The energy density in these oscillations redshifts as a^{-3} , therefore after a single Hubble time it reduces by e^{-3} , more than an order of magnitude. Being incomplete, typical timescales of bubble evolution are larger than $10H^{-1}$, so a duration of few Hubble times may be regarded as short. We therefore do not need to impose any further condition, and the oscillations decay quickly.

To summarize, the potential given by Eq. (A1) satisfies our assumptions about the model in the following parameter range:

$$\frac{9\sqrt{\lambda_4}}{2\lambda_3}H \lesssim m_\chi \lesssim \min\left(H, \frac{\lambda_3\sqrt{M_{\rm pl}H}}{\lambda_4^{3/4}}\right), \qquad (A8)$$

$$\lambda_4 \ll \lambda_3^2$$
. (A9)

The second condition ensures that the first can be satisfied in a wide range of masses, making the model viable in a significant portion of the parameter range.

1. Gravitational wave signal

We have shown the potential satisfies the assumptions made in this work, and now we apply our results and calculate the gravitational wave amplitude. Below, we discuss how our assumption regarding reheating may impose constraints on additional parameters, but the predicted signal is independent of those constraints.

The Hawking-Moss tunneling rate per unit volume can be calculated by neglecting the quartic term [51]:

$$\frac{\Gamma}{V} = \frac{m_{\chi}^2 H^2}{8\pi^2} \exp\left(-\frac{4\pi^2 m_{\chi}^4}{9H^4 \lambda_3^2}\right). \tag{A10}$$

The inflaton velocity $\dot{\phi}$ can be related to H by using CMB spectral amplitude measurements [16]. Assuming $\dot{\phi}$ and H do not significantly change after CMB modes exit the horizon, we have $\dot{\phi}^2 \approx 10^{11} H^4$ and the parameter $\gamma_{\rm PT}$ defined in the main text is given by

$$\gamma_{\rm PT} \approx \frac{1}{H^4} \frac{\Gamma}{V} \left(\frac{\Delta V_{\rm PT}}{10^{11} H^4} \right)^2.$$
(A11)

The gravitational wave amplitude can now be calculated directly from the parameters of the potential by plugging Eqs. (A3), (A10), and (A11) into Eq. (18). Taking the same parameters used to produce Fig. 6 above, $m_{\chi}=0.4H$, $\lambda_3=0.3$ and $\lambda_4=2\times10^{-4}$, we find

$$\frac{d\Omega_{\rm GW}}{d\log k} \approx 6.6 \times 10^{-8},\tag{A12}$$

a detectable amplitude relevant for a wide range of detectors. In Fig. 7 we fix the mass $m_\chi = 0.4 H$ and visualize the coupling space where gravitational waves are experimentally relevant, $10^{-15} < \frac{d\Omega_{\rm GW}}{d\log k} < 10^{-5}$. As shown in the figure, the gravitational wave amplitude is within a relevant detection range without fine tuning of the model parameters. In the gray region, the lower bound on m_χ from Eq. (A8) is violated, meaning the step function approximation is invalid. In this regime, the model may still produce gravitational waves, but our calculation becomes inaccurate.

2. Reheating

Finally, the transition was assumed to complete everywhere once the universe reheats, due to either the slower expansion rate or finite temperature effects. For the Hawking-Moss transition discussed here, the latter is more relevant since the zero-temperature Hawking-Moss

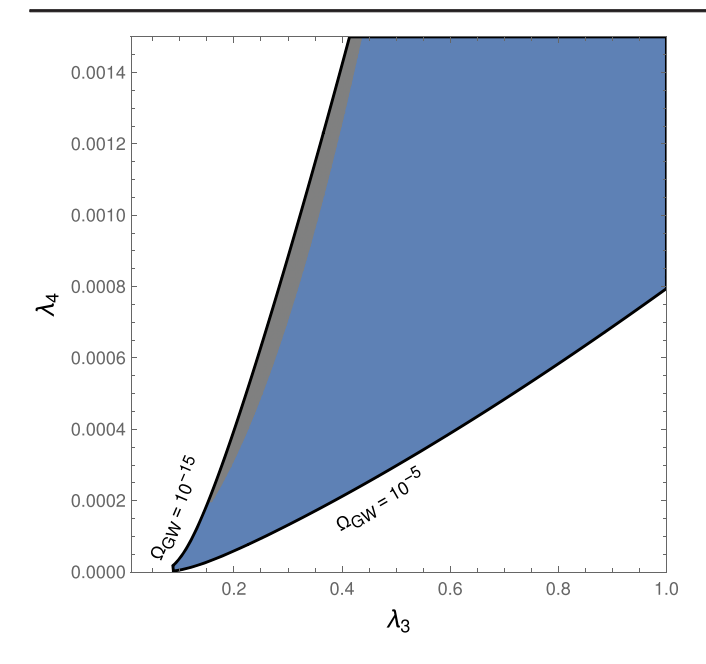


FIG. 7. The parameter range where the peak GW amplitude $\frac{d\Omega_{\rm GW}}{d\log k}$ is between 10^{-5} and 10^{-15} . The mass is $m_\chi=0.4H$, satisfying the inequalities of Eq. (A8) in the blue region. In the gray region, the "quick rolling" condition of Eq. (A7) is violated, making the result inaccurate.

tunneling rate decays quickly with the expansion rate, see Eq. (A10). The local minimum of χ will be destabilized at reheating if χ thermalizes with sufficiently high temperature. To show this is possible, we write a concrete reheating model.

We assume once the inflaton ϕ ends its slow-rolling, it oscillates and decays entirely into χ particles that may subsequently decay into other particles. The decay is enabled by adding the coupling

$$V_{\rm RH} = \frac{m_{\phi} \lambda_{\phi \chi}}{2} \phi \chi^2, \tag{A13}$$

where m_{ϕ} is the inflaton mass, assumed to satisfy $m_{\phi} \gg H$ at reheating.

We require the potential given in Eq. (A1) to remain unchanged during inflation by imposing $m_{\phi, \text{SR}} \lambda_{\phi\chi} \Delta \phi \ll m_\chi^2$, where $m_{\phi, \text{SR}}$ is the inflaton mass in the slow-roll regime of its potential and $\Delta \phi$ the distance it travels. Using $\Delta \phi = H N \dot{\phi}$, with $N \approx 40$ e-folds of slow-roll and $\dot{\phi} \approx 10^{11} H$ as above, we find $\Delta \phi \approx 1.25 \times 10^7 H$. The squared mass $m_{\phi, \text{SR}}^2$ is determined by the second slow-roll parameter η_V , which can be estimated as -0.01 [16]. Putting these numbers together, along with $m_\chi = 0.4 H$, we find that imposing the condition

$$\lambda_{\phi\gamma} \lesssim 7.5 \times 10^{-8} \tag{A14}$$

guarantees the potential in Eq. (A13) to be negligible compared to (A1).⁴

The decay rate of a ϕ particle is given for $m_{\phi} \gg m_{\chi}$ (assumed to be true at reheating) by

$$\Gamma_{\phi \to \chi \chi} = \frac{\lambda_{\phi \chi}^2 m_{\phi}}{16\pi},\tag{A15}$$

and the corresponding reheating temperature is $T_{\rm RH} \approx 1.23 \sqrt{M_{\rm pl} \Gamma_{\phi \to \chi \chi}}$. This temperature is required to be higher than m_χ in order to destabilize the false vacuum. For example, choosing $\lambda_{\phi \chi} = 7 \times 10^{-8}$ and $m_\phi = 10 H$, with $H = 10^{-16} M_{\rm pl}$ as above, we find a reheating temperature or $T_{\rm RH} = 3.84 H$. We calculated the effective potential at that temperature using the optimized partial dressing scheme [59], the result is shown in orange in Fig. 5. As the figure shows, this temperature is sufficiently high to destabilize the false vacuum. Increasing m_ϕ/H or decreasing H will make $T_{\rm RH}/H$ higher, making the parameter range where the false vacuum is unstable at reheating very large.

APPENDIX B: THE 2-POINT CORRELATION FUNCTION OF THE TUNNELING TIME

Here we calculate the correlation function of $\delta t_{\vec{x}}$ defined by Eq. (13),

$$\langle \delta t_{\vec{x}} \delta t_{\vec{x}'} \rangle = \langle t_{\vec{x}} t_{\vec{x}'} \rangle - \langle t_{\vec{x}} \rangle^2 \tag{B1}$$

as a function of $r = |\vec{x} - \vec{x}'|$. For simplicity, we will ignore the end of inflation for now, and calculate the correlation as if inflation goes on forever. In the next section, we will show how the calculation has to be modified in order to account for the end of inflation.

After deriving the detailed correlation function, we find a simple approximate expression valid under the assumption of slow tunneling rate, $\Gamma/V \ll H^4$. This simplification will come handy in the next section where we compute the effect of non-Gaussianity.

1. The correlation without ending inflation

To compute the correlation function, we first need to find the probability distribution for the decay of the false vacuum. For a general phase transition, the probability to find a given point in space in the false vacuum by the time t is given by [50]

$$p(t_{\vec{x}} > t) = e^{-I(t)} \tag{B2}$$

⁴We checked that the effect of $V_{\rm RH}$ on the slow-roll potential of ϕ is negligible, as well as the loop corrections to the mass of χ .

with,

$$I(t) = \frac{4\pi}{3} \int_{t_0}^{t} dt' \frac{\Gamma}{V}(t') a^3(t') r^3(t, t').$$
 (B3)

Here I(t) is the ratio of the space volume inside the bubbles over the entire volume at time t, without accounting for the overlaps. The latter are automatically taken care of by the exponent in Eq. (B2). Note that by definition, Eq. (B2) is the complementary cumulative probability. In Eq. (B3), r(t,t') is the comoving radius of a bubble that was created at time t' and measured at time t. $\frac{\Gamma}{V}(t')$ is the tunneling rate per unit volume at time t', and t_0 the time when the phase transition commences. We will take $t_0 = 0$ to simplify the expressions.

For the toy models studied in this work, Γ/V is constant. We further assume that at formation, the bubble radius coincides with the Hubble radius and thus,

$$r(\mathbf{t}, \mathbf{t}') = \left(a_0 e^{H\mathbf{t}'} H\right)^{-1} \equiv r_{\mathcal{H}}(\mathbf{t}'), \tag{B4}$$

where a_0 is the scale factor at t = 0. We stress that this expression is exact for the case of the HM transition, but is only approximate for the CdL transition. In the latter case, we neglect the time it takes the bubble to grow to horizon-size. Plugging the radius back into Eq. (B3) gives the exponential decay

$$p(t_{\vec{x}} > t) = e^{-t/\tau}, \tag{B5}$$

with τ being the mean lifetime of the false vacuum at any given point

$$\tau = \left[\frac{4\pi}{3} \left(\frac{1}{H^3}\right) \left(\frac{\Gamma}{V}\right)\right]^{-1}.$$
 (B6)

which agrees with a more direct calculation.

Now the second term in Eq. (B1) can be extracted by taking the mean of the probability at Eq. (B5):

$$\langle t_{\vec{\mathbf{r}}} \rangle = \tau.$$
 (B7)

The remaining part of this section is focused on computing the covariance $\langle t_{\vec{x}}t_{\vec{x}'}\rangle$. We use the law of total expectation

$$\langle t_{\vec{x}}t_{\vec{x}'}\rangle = \langle t_{\vec{x}}E(t_{\vec{x}'}|t_{\vec{x}})\rangle, \tag{B8}$$

where $E(\cdot)$ is the conditional expectation value. Applying this to the exponential probability distribution described by Eq. (B5) gives

$$\langle t_{\vec{x}}t_{\vec{x}'}\rangle = \frac{1}{\tau} \int_0^\infty dt_{\vec{x}}t_{\vec{x}}e^{-t_{\vec{x}}/\tau}E(t_{\vec{x}'}|t_{\vec{x}}). \tag{B9}$$

With the above, we are left with computing the conditional expectation value, $E(t_{\vec{x}'}|t_{\vec{x}})$. This describes the

expectation of $t_{\vec{x}'}$ assuming we know $t_{\vec{x}}$. Given the cumulative probability distribution in the domain of $(0, +\infty)$, the expectation is given by

$$E(t_{\vec{x}}|t_{\vec{x}}) = \int_0^\infty dt \, p(t_{\vec{x}'} > t|t_{\vec{x}}). \tag{B10}$$

To compute Eq. (B9), we separate the integral over $t_{\vec{x}}$ into two intervals, $t_{\vec{x}} \in [0, t_s)$ and $t_{\vec{x}} \in [t_s, \infty)$, where t_s is the separation time, defined to be the moment when the distance between \vec{x} and \vec{x}' becomes larger than twice the Hubble radius, i.e. $r = 2r_{\mathcal{H}}(t_s)$. One finds,

$$t_{\rm s} = \frac{1}{H} \log \frac{2}{a_0 H r}.\tag{B11}$$

When the points are more than two radii apart, they can no longer be contained inside any single bubble, and thus t_s represents the moment at which these two points became independent.

a. First interval: $0 < t_{\vec{x}} < t_{\rm s}$

Let us first consider the case where the false vacuum at \vec{x} decays before the two points are causally disconnected. In principle a bubble that contains \vec{x}' may form at any time t. To evaluate the integral in Eq. (B10), we further break it into two intervals, $0 \le t < t_{\vec{x}}$ and $t \ge t_{\vec{x}}$. We begin with the first interval.

In the case where $t < t_{\vec{x}}$, the bubble cannot contain \vec{x} . We therefore have to modify Eq. (B3) in order exclude from I the contribution of bubbles which form at $t < t_{\vec{x}}$ and include \vec{x} . The centers of all possible bubbles that could form at t containing \vec{x}' form a ball of radius $r_{\mathcal{H}}(t)$ centered at \vec{x}' . Similarly, the centers of bubbles containing \vec{x} form a Hubble ball of the same radius centered at \vec{x} . Therefore, if we randomly draw a bubble that contains \vec{x}' , the probability this bubble does not contain \vec{x} is given by the fraction of the Hubble ball centered at \vec{x}' that does not overlap with the ball centered at \vec{x} :

$$f_V(t) = \frac{V_H(t) - V_O(t)}{V_H(t)} = \frac{3r}{4r_H(t)} - \frac{r^3}{16r_H^3(t)},$$
 (B12)

where the Hubble volume is $V_{\mathcal{H}} = 4\pi r_{\mathcal{H}}(t)^3/3$ and the overlapping volume is $V_{\rm O} = \pi (4r_{\mathcal{H}}(t) + r)(2r_{\mathcal{H}}(t) - r)^2/12$. Now, excluding from (B3) the bubbles that include \vec{x} means replacing I(t) with

$$J(t) = \frac{4\pi}{3} \int_0^t dt' \frac{\Gamma}{V} a^3(t') r_{\mathcal{H}}^3(t') f_V(t')$$
$$= \frac{1}{\tau H} \left(\frac{3r}{4r_{\mathcal{H}}(t')} - \frac{r^3}{48r_{\mathcal{H}}^3(t')} \right) \Big|_{t'=0}^{t'=t}.$$
(B13)

For $t < t_{\vec{x}}$, the probability is thus given by,

$$p(t_{\vec{x}'} > t | t_{\vec{x}}) = e^{-J(t)}.$$
 (B14)

We move on to the interval $t \ge t_{\vec{x}}$. At $t = t_{\vec{x}}$, we know a bubble forms around \vec{x} . To compute the probability this bubble does not include \vec{x}' let us first map out the allowed region for the bubble center. To contain \vec{x} the bubble center can be placed anywhere in a sphere that is centered at \vec{x} with a radius of $r_{\mathcal{H}}(t_{\vec{x}})$. To avoid containing \vec{x}' , the center of the bubble cannot be anywhere inside a sphere centered at \vec{x}' with radius $r_{\mathcal{H}}(t_{\vec{x}'})$. Therefore, if we randomly place a bubble such that it contains \vec{x} , the probability it does not contain \vec{x}' is given by the nonoverlapping fraction $f_V(t_{\vec{x}})$. As a result, the probability that \vec{x}' will remain in the false vacuum when the bubble around \vec{x} is formed, is given by

$$p(t_{\vec{x}'} > t_{\vec{x}}|t_{\vec{x}}) = e^{-J(t_{\vec{x}})} f_V(t_{\vec{x}}).$$
 (B15)

We note that the discontinuity of $p(t_{\vec{x}'} > t | t_{\vec{x}})$ at $t = t_{\vec{x}}$ [see Eqs. (B14) and (B15)], is due to the instantaneous formation of a bubble at \vec{x} .

The known value of $t_{\bar{x}}$ does not pose any constraints on bubble formation after $t_{\bar{x}}$, so for $t > t_{\bar{x}}$ the probability will decay exponentially with the same rate as in Eq. (B5):

$$p(t_{\vec{x}'} > t | t_{\vec{x}}) = e^{-J(t_{\vec{x}})} f_V(t_{\vec{x}}) e^{-(t - t_{\vec{x}})/\tau}.$$
 (B16)

Finally, putting Eqs. (B14) and (B16) into Eq. (B10) we obtain the conditional expectation

$$E(t_{\vec{x}'}|t_{\vec{x}}) = \int_0^{t_{\vec{x}}} e^{-J(t)} dt + \tau e^{-J(t_{\vec{x}})} f_V(t_{\vec{x}}) \quad (B17)$$

b. Second interval: $t_{\vec{x}} \geq t_s$

This corresponds to the scenario where the false vacuum at \vec{x} decays after the two bubbles are causally disconnected. For $t < t_s$ the probability is given by Eq. (B14) as before. At t_s the two points become separated and the decay becomes independent. Therefore, $t_{\vec{x}}$ is irrelevant to the conditional probability. The cumulative distribution function is given by

$$p(t_{\vec{x}'} > t | t_{\vec{x}}) = \begin{cases} e^{-J(t)}, & t < t_{s} \\ e^{-J(t_{s})} e^{-(t-t_{s})/\tau}, & t \ge t_{s} \end{cases}$$
(B18)

which means the conditional expectation is

$$E(t_{\vec{x}'}|t_{\vec{x}}) = \int_0^{t_s} e^{-J(\mathbf{t})} dt + \tau e^{-J(t_s)}.$$
 (B19)

Since Eq. (B19) is independent of $t_{\vec{x}}$, it can be integrated analytically when plugged back into Eq. (B9).

Putting both intervals back into Eq. (B9) we reach the final expression for the two-point expectation value:

$$\langle t_{\vec{x}} t_{\vec{x}'} \rangle = \frac{1}{\tau} \int_0^{t_s} dt_{\vec{x}} t_{\vec{x}} e^{-t_{\vec{x}}/\tau} E(t_{\vec{x}'} | t_{\vec{x}})$$

$$+ \left[\int_0^{t_s} e^{-J(t)} dt + e^{-J(t_s)} \tau \right] e^{-t_s/\tau} (t_s + \tau), \quad (B20)$$

where in the first term we plug in Eq. (B17) and integrate numerically. This result is only valid for $t_{\rm s} > 0$. If $t_{\rm s} \le 0$, the points were separated before the phase transition started, so they decay independently and $\langle \delta t_{\rm r} \delta t_{\rm r'} \rangle = 0$.

2. Adding the end time of inflation

Now, we have to repeat the above calculation, taking into account the end of inflation at $t_{\rm e}=t_{\rm reheating}$, when reheating starts. As discussed in the main text, we assume that all of the volume of space which remained in the false vacuum will move to the true vacuum immediately at $t_{\rm e}$, which means the probability distribution Eq. (B5) has to be replaced with

$$p(t_{\vec{x}} > t) = \begin{cases} e^{-t/\tau}, & t < t_{e} \\ 0, & t \ge t_{e} \end{cases}$$
 (B21)

and the corresponding expectation value Eq. (B7) is replaced with

$$\langle t_{\vec{x}} \rangle = \tau (1 - e^{-t_{\rm e}/\tau}). \tag{B22}$$

Note that having an end of inflation is similar to putting a regulator to $\langle t_{\vec{x}} \rangle$. Without t_e the expected transition time τ diverges in the slow tunneling limit $(\Gamma/(VH^4) \to 0)$. With the new probability distribution given in Eq. (B21), the expectation approaches t_e in the limit of slow tunneling.

The law of total expectation can be applied in the same manner as above, but now the integral in Eq. (B9) ends at t_e :

$$\langle t_{\vec{x}}t_{\vec{x}'}\rangle = \frac{1}{\tau} \int_0^{t_e} dt_{\vec{x}}t_{\vec{x}}e^{-t_{\vec{x}}/\tau}E(t_{\vec{x}'}|t_{\vec{x}}) + t_e e^{-t_e/\tau}E(t_{\vec{x}'}|t_e),$$
(B23)

where the second term accounts for the finite probability that \vec{x} does not tunnel until the end of inflation, $P(t_{\vec{x}} = t_e) = e^{-t_e/\tau}$.

The derivation of the conditional expectation is the same as in the previous section, except for the fact that the integrals end at t_s instead of ∞ . We are only interested in scales which exited the horizon before the end of inflation, which means $t_s < t_e$. Under this assumption, we split the conditional expectation to two cases as above, $t_{\vec{x}} < t_s$ and $t_s < t_{\vec{x}} \le t_e$. In the first case, Eqs. (B14) and (B16) remain

unchanged, but the integral over t ends at t_e , which means Eq. (B17) has to be replaced with

$$E(t_{\vec{x}'}|t_{\vec{x}}) = \int_0^{t_{\vec{x}}} e^{-J(t)} dt + e^{-J(t_{\vec{x}})} f_V(t_{\vec{x}}) \tau \left(1 - e^{-(t_e - t_{\vec{x}})/\tau}\right).$$
(B24)

Similarly, Eq. (B19) has to be replaced with

$$E(t_{\vec{x}'}|t_{\vec{x}}) = \int_0^{t_s} e^{-J(t)} dt + e^{-J(t_s)} \tau \left(1 - e^{-(t_c - t_s)/\tau}\right). \quad (B25)$$

Equations (B24) and (B25) can be plugged into Eq. (B23) and integrated numerically to get the required correlation $\langle t_{\vec{x}} t_{\vec{x}'} \rangle$.

3. The small Γ/V limit

The above derivation allows the 2-point correlation to be calculated without assuming anything about Γ . Here, we derive a simpler closed-form formula by assuming $\Gamma/(VH^3) \ll t_{\rm e}^{-1}$. This assumption makes the resulting power spectrum linear in Γ , and the approximation will be used in the next section to show that non-Gaussianity can be ignored when calculating the GW spectrum.

Once again, we denote by $t_{\rm s}$ the moment at which the points \vec{x} and \vec{x}' become causally separated, and consider the case in which the two points we are looking at were separated before the end of inflation, $t_{\rm s} < t_{\rm e}$. Since the rate of bubble nucleation is very small, the probability that more than a single bubble formed around any of the two points before the separation time $t_{\rm s}$, can be neglected. The correlation of $\delta t_{\vec{x}}$ can therefore be written as

$$\langle \delta t_{\vec{x}} \delta t_{\vec{x}'} \rangle$$

$$= E \left(\delta t_{\vec{x}} \delta t_{\vec{x}'} \middle| \begin{array}{c} \text{bubble with both} \\ \text{points before } t_s \end{array} \right) P \left(\begin{array}{c} \text{bubble with both} \\ \text{points before } t_s \end{array} \right) P \left(\begin{array}{c} \text{bubble with both} \\ \text{points before } t_s \end{array} \right) P \left(\begin{array}{c} \text{bubble with} \\ \text{only } \vec{x} \text{ before } t_s \end{array} \right) P \left(\begin{array}{c} \text{bubble with} \\ \text{only } \vec{x} \text{ before } t_s \end{array} \right) P \left(\begin{array}{c} \text{bubble with} \\ \text{only } \vec{x}' \text{ before } t_s \end{array} \right) P \left(\begin{array}{c} \text{bubble with} \\ \text{only } \vec{x}' \text{ before } t_s \end{array} \right) P \left(\begin{array}{c} \text{bubble with} \\ \text{only } \vec{x}' \text{ before } t_s \end{array} \right) P \left(\begin{array}{c} \text{bubble with} \\ \text{only } \vec{x}' \text{ before } t_s \end{array} \right) P \left(\begin{array}{c} \text{bubble with} \\ \text{only } \vec{x}' \text{ before } t_s \end{array} \right) P \left(\begin{array}{c} \text{bubble with} \\ \text{only } \vec{x}' \text{ before } t_s \end{array} \right) P \left(\begin{array}{c} \text{bubble with} \\ \text{only } \vec{x}' \text{ before } t_s \end{array} \right) P \left(\begin{array}{c} \text{bubble with} \\ \text{only } \vec{x}' \text{ before } t_s \end{array} \right) P \left(\begin{array}{c} \text{bubble with} \\ \text{only } \vec{x}' \text{ before } t_s \end{array} \right) P \left(\begin{array}{c} \text{bubble with} \\ \text{only } \vec{x}' \text{ before } t_s \end{array} \right) P \left(\begin{array}{c} \text{bubble with} \\ \text{only } \vec{x}' \text{ before } t_s \end{array} \right) P \left(\begin{array}{c} \text{bubble with} \\ \text{only } \vec{x}' \text{ before } t_s \end{array} \right) P \left(\begin{array}{c} \text{bubble with} \\ \text{only } \vec{x}' \text{ before } t_s \end{array} \right) P \left(\begin{array}{c} \text{bubble with} \\ \text{only } \vec{x}' \text{ before } t_s \end{array} \right) P \left(\begin{array}{c} \text{bubble with} \\ \text{only } \vec{x}' \text{ before } t_s \end{array} \right) P \left(\begin{array}{c} \text{bubble with} \\ \text{only } \vec{x}' \text{ before } t_s \end{array} \right) P \left(\begin{array}{c} \text{bubble with} \\ \text{only } \vec{x}' \text{ before } t_s \end{array} \right) P \left(\begin{array}{c} \text{bubble with} \\ \text{only } \vec{x}' \text{ before } t_s \end{array} \right) P \left(\begin{array}{c} \text{bubble with} \\ \text{only } \vec{x}' \text{ before } t_s \end{array} \right) P \left(\begin{array}{c} \text{bubble with} \\ \text{only } \vec{x}' \text{ before } t_s \end{array} \right) P \left(\begin{array}{c} \text{bubble with} \\ \text{before } t_s \end{array} \right) P \left(\begin{array}{c} \text{bubble with} \\ \text{before } t_s \end{array} \right) P \left(\begin{array}{c} \text{bubble with} \\ \text{before } t_s \end{array} \right) P \left(\begin{array}{c} \text{bubble with} \\ \text{before } t_s \end{array} \right) P \left(\begin{array}{c} \text{bubble with} \\ \text{before } t_s \end{array} \right) P \left(\begin{array}{c} \text{bubble with} \\ \text{before } t_s \end{array} \right) P \left(\begin{array}{c} \text{bubble with} \\ \text{before } t_s \end{array} \right) P \left(\begin{array}{c} \text{bubble with} \\ \text{before } t_s \end{array} \right) P \left(\begin{array}{c} \text{bubble with} \\ \text{bubble with} \\ \text{befo$$

We now show that in the $\Gamma/V \ll H^4$ limit, the first term in Eq. (B26) becomes linear in Γ/V , while the other three terms are of order $(\Gamma/V)^2$.

Consider first the last term. Since the points become independent after t_s , the expectation value in the that term can be written as

$$E\left(\delta t_{\vec{x}} \delta t_{\vec{x}'} \middle| \begin{array}{c} \text{no bubble} \\ \text{before } t_s \end{array}\right) = E(\delta t_{\vec{x}} | t_{\vec{x}} > t_s)^2.$$
 (B27)

This expectation can be calculated by integrating the probability distribution given in Eq. (B21) from t_s to t_e ,

$$E(\delta t_{\vec{x}}|t_{\vec{x}} > t_{s}) = t_{s} + \tau e^{-t_{e}/\tau} (1 - e^{t_{s}/\tau})$$

$$= \frac{t_{s}}{\tau} (t_{e} - t_{s}/2) + \mathcal{O}((t_{s}/\tau)^{2}).$$
 (B28)

Together with Eq. (B6), this result shows the last term in Eq. (B26) is at least of order $(\Gamma/V)^2$. Similarly, the expectation value in the second and third terms can be factorized, e.g.,

$$E\left(\delta t_{\vec{x}} \delta t_{\vec{x}'} \middle| \begin{array}{c} \text{bubble with} \\ \text{only } \vec{x}' \text{ before } t_s \end{array}\right)$$

$$= E\left(\delta t_{\vec{x}'} \middle| \begin{array}{c} \text{bubble with} \\ \text{only } \vec{x}' \text{ before } t_s \end{array}\right) E\left(\delta t_{\vec{x}} \middle| t_{\vec{x}} > t_s \right), \quad (B29)$$

and Eq. (B28) implies that the second factor is linear in Γ/V . Since the first factor is regular in Γ/V , the whole expression is at least linear in Γ/V . Given that the probabilities of forming a bubble are also linear in Γ/V , the second and third terms of Eq. (B26) must be at least of order $(\Gamma/V)^2$.

Finally, we are ready to calculate the dominant term: the contribution to the correlation from a single bubble forming around both points. This contribution can be rewritten as

$$\int_{0}^{t_{s}} E\left(\delta t_{\vec{x}} \delta t_{\vec{x}'} \middle| \begin{array}{c} \text{bubble with} \\ \text{both points at t} \end{array}\right) dP\left(\begin{array}{c} \text{bubble with} \\ \text{both points at t} \end{array}\right)$$

$$= \int_{0}^{t_{s}} (t - \langle t_{\vec{x}} \rangle)^{2} \frac{\Gamma}{V} V_{\text{overlap}}(t) dt \tag{B30}$$

where $dP \propto \Gamma dt$ is the probability of forming a bubble in the infinitesimal time interval dt, and $V_{\text{overlap}}(t)$ is the physical volume of overlap between two Hubble spheres, each centered at \vec{x} and \vec{x}' . The expectation value $\langle t_{\vec{x}} \rangle$ is given by Eq. (B22), but since we are calculating only the first order in Γ we can take $\langle t_{\vec{x}} \rangle \simeq t_{\text{e}}$. From this point, it is straightforward to write V_{overlap} explicitly and integrate Eq. (B30) directly. Instead, we introduce a trick that will be useful later. The overlap volume between two spheres can be written as an integral over a δ function:

$$V_{\text{overlap}}(t) = a^{3}(t) \int_{r_{\mathcal{H}}} d^{3}y_{1} \int_{r_{\mathcal{H}}} d^{3}y_{2} \delta(\vec{y}_{1} - \vec{y}_{2} + \vec{r})$$
 (B31)

where both integrals are over a sphere of radius $r_{\mathcal{H}}$ centered at the origin, and $\vec{r} = \vec{x}_1 - \vec{x}_2$ is the separation between the centers of the overlapping spheres. This expression automatically vanishes for $t > t_s$, so the upper limit of the integral in Eq. (B30) can be replaced with ∞ . After doing so, the only dependence of

Eq. (B30) on \vec{x}_1 and \vec{x}_2 is through \vec{r} in the δ function. That makes taking the Fourier transform trivial,

$$\langle \delta t_{\vec{k}_1} \delta t_{\vec{k}_2} \rangle = \delta(\vec{k}_1 + \vec{k}_2) \left(\frac{12\pi}{k^2} \right) \times \frac{1}{\tau H} \int_0^\infty \frac{dt}{a(t)} \left(t - \langle t_{\vec{k}} \rangle \right)^2 j_1^2 (k r_{\mathcal{H}}) \quad (B32)$$

where $j_1(x) = \frac{1}{x}(\frac{\sin x}{x} - \cos x)$ is the first spherical Bessel function. Using $a(t) = a_0 e^{Ht}$ and $r_{\mathcal{H}}(t) = (Ha(t))^{-1}$ the integral can be evaluated numerically, and by comparing with Eqs. (13) and (14) we can extract the spectrum $\mathcal{P}_{\mathcal{R}}$. This result is in agreement with the full calculation of the previous section in the $\Gamma/V \to 0$ limit.

APPENDIX C: ALLEVIATING THE ASSUMPTION OF CONSTANT $\dot{\phi}$ AND H

In deriving Eq. (13) from Eq. (12), we assumed $H/\dot{\phi}^2$ to be constant, which resulted with \mathcal{R} being a linear function of $t_{\vec{x}}$. This result meant we only have to calculate correlations of the tunneling times $t_{\vec{x}}$, and then convert the final results to correlations of \mathcal{R} with the use of Eq. (13). We will now discuss how the spectrum can be approximated without this simplification.

 \mathcal{R} is obtained by integrating Eq. (12) over t, with an initial condition of $\mathcal{R}=0$. The theta functions in Eq. (7) ensure the integrand vanishes unless t is between $\langle t_{\vec{x}} \rangle$ and $t_{\vec{x}}$, allowing us to write the integral as

$$\mathcal{R}(t_{\vec{x}}) = -\Delta V_{\text{PT}} \int_{\langle t_{\vec{x}} \rangle}^{t_{\vec{x}}} \frac{H}{\dot{\phi}^2} dt. \tag{C1}$$

Equation (13) can be recovered from this more general result by assuming the integrand is constant.

As we have shown in Appendix B 3, in the limit of small Γ/V we only have to consider the contribution of a single bubble to the correlation function, given by Eq. (B30). Assuming $\mathcal{R}(t_{\vec{x}})$ is a well-behaved function, the approximation is still valid, but we have to modify Eq. (B30) to calculate the correlation of \mathcal{R} directly instead of using $\delta t_{\vec{x}}$:

$$\int_{0}^{t_{s}} E\left(\mathcal{R}_{\vec{x}}\mathcal{R}_{\vec{x}'}\right| \begin{array}{c} \text{bubble with} \\ \text{both points at t} \end{array}\right) dP\left(\begin{array}{c} \text{bubble with} \\ \text{both points at t} \end{array}\right)$$
$$= \int_{0}^{t_{s}} \mathcal{R}(t)^{2} \frac{\Gamma}{V} V_{\text{overlap}}(t) dt. \tag{C2}$$

This result can be used to calculate the scalar spectrum for a general inflationary background, but only in the limit of small Γ/V .

Let us now consider a concrete example to demonstrate how the spectral shape can be affected by the time dependence of $\frac{H}{\phi^2}$. In this example, $\frac{H}{\phi^2}$ starts at some value $\frac{H}{\phi^2}$, and

remains constant until t_{drop} , when it instantly changes to a new value smaller from the original one by a factor of 10. In that scenario, the integrand of Eq. (C1) can be written as

$$\frac{H}{\dot{\phi}^2} = \frac{H}{\dot{\phi}_0^2} \left[\theta(t_{\text{drop}} - t) + \frac{1}{10} \theta(t - t_{\text{drop}}) \right], \quad (C3)$$

and after integrating it, we get

$$\mathcal{R}(t_{\vec{x}}) = -\frac{H\Delta V_{\text{PT}}}{\dot{\phi}_0^2} \begin{cases} t_{\vec{x}} - t_{\text{drop}} + \frac{1}{10} (t_{\text{drop}} - \langle t_{\vec{x}} \rangle), & t_{\vec{x}} < t_{\text{drop}} \\ \frac{1}{10} (t_{\vec{x}} - \langle t_{\vec{x}} \rangle), & t_{\vec{x}} \ge t_{\text{drop}} \end{cases}$$
(C4)

The colored lines in Fig. 3 were calculated by plugging this result into (C2).

APPENDIX D: NON-GAUSSIANITY AND THE INDUCED GRAVITATIONAL WAVES

Here, we very briefly review the equations necessary for calculating the secondary gravitational waves, taken from [45,60]. We then use the methods of the previous section to calculate the four-point correlation function and show that Eq. (16) can be applied to our model, ignoring non-Gaussianity.

1. The induced gravitational waves

To calculate the gravitational wave spectrum, we need the four-point correlation function of \mathcal{R} . In the general, non-Gaussian case the correlation can be split into disconnected and connected components [60]:

$$\begin{split} \left\langle \mathcal{R}_{\vec{k}_1} \mathcal{R}_{\vec{k}_2} \mathcal{R}_{\vec{k}_3} \mathcal{R}_{\vec{k}_4} \right\rangle &= \left\langle \mathcal{R}_{\vec{k}_1} \mathcal{R}_{\vec{k}_2} \mathcal{R}_{\vec{k}_3} \mathcal{R}_{\vec{k}_4} \right\rangle_{d} \\ &+ \left\langle \mathcal{R}_{\vec{k}_1} \mathcal{R}_{\vec{k}_2} \mathcal{R}_{\vec{k}_3} \mathcal{R}_{\vec{k}_4} \right\rangle_{c}. \end{split} \tag{D1}$$

The disconnected part satisfies Wick's theorem,

$$\begin{split} \left\langle \mathcal{R}_{\vec{k}_1} \mathcal{R}_{\vec{k}_2} \mathcal{R}_{\vec{k}_3} \mathcal{R}_{\vec{k}_4} \right\rangle_{\mathrm{d}} &= \left\langle \mathcal{R}_{\vec{k}_1} \mathcal{R}_{\vec{k}_2} \right\rangle \left\langle \mathcal{R}_{\vec{k}_3} \mathcal{R}_{\vec{k}_4} \right\rangle + \left\langle \mathcal{R}_{\vec{k}_2} \mathcal{R}_{\vec{k}_3} \right\rangle \\ &\times \left\langle \mathcal{R}_{\vec{k}_4} \mathcal{R}_{\vec{k}_1} \right\rangle + \left\langle \mathcal{R}_{\vec{k}_1} \mathcal{R}_{\vec{k}_3} \right\rangle \left\langle \mathcal{R}_{\vec{k}_2} \mathcal{R}_{\vec{k}_4} \right\rangle, \end{split} \tag{D2}$$

and the connected part defines the connected trispectrum \mathcal{T} ,

$$\langle \mathcal{R}_{\vec{k}_1} \mathcal{R}_{\vec{k}_2} \mathcal{R}_{\vec{k}_3} \mathcal{R}_{\vec{k}_4} \rangle_{c} = \delta^{3} (\vec{k}_1 + \vec{k}_2 + \vec{k}_3 + \vec{k}_4)
\times \mathcal{T} (\vec{k}_1, \vec{k}_2, \vec{k}_3, \vec{k}_4).$$
(D3)

In the Gaussian case, the connected part vanishes because of Wick's theorem and the four-point correlation function is fully described by the scalar spectrum defined by Eq. (14).

The GW spectrum induced by the disconnected part is given by Eq. (16), where $\tilde{I}(v, u, k\eta)$ is a Green's function integral that was calculated analytically in [45,46]. Since we are only interested in the energy density of gravitational waves today, we only need the late-time oscillation average of \tilde{I}^2 , which, during radiation domination, is given by

$$\overline{\tilde{I}^{2}(v, u, k\eta \to \infty)} = \frac{1}{2} \left(\frac{3(u^{2} + v^{2} - 3)}{4u^{3}v^{3}k\eta} \right)^{2} \left[\left(-4uv + \left(u^{2} + v^{2} - 3 \right) \log \left| \frac{3 - (u + v)^{2}}{3 - (u - v)^{2}} \right| \right)^{2} + \pi^{2} (u^{2} + v^{2} - 3)^{2} \Theta(v + u - \sqrt{3}) \right].$$
(D4)

The connected contribution to the GW spectrum is⁵

$$\mathcal{P}_{\lambda_4}(k)|_{c} = \frac{k^3}{\pi^5} \int d^3 q_1 d^3 q_2 Q_{\lambda_4}(\vec{k}, \vec{q}_1) Q_{\lambda_4}(\vec{k}, \vec{q}_2) I(|\vec{k} - \vec{q}_1|, q_1, \eta) I(|\vec{k} - \vec{q}_2|, q_2, \eta) \mathcal{T}(\vec{q}_1, \vec{k} - \vec{q}_1, -\vec{q}_2, \vec{q}_2 - \vec{k}), \quad (D5)$$

where the Q_{λ_4} are polarization factors, given by

$$Q_{\lambda_4}(\vec{k}, \vec{q}) \equiv \epsilon_{ij}^{\lambda_4}(\vec{k}) q_i q_j, \tag{D6}$$

where $\epsilon_{ij}^{\lambda_4}$ with $\lambda_4=+,\times$ is a basis of traceless transverse polarization tensors. I in Eq. (D5) is related to \tilde{I} used above through a change of variables, $\tilde{I}(v,u,x)\equiv k^2I(vk,uk,x/k)$. Taking \vec{k} to be in the z direction and writing \vec{q} in spherical coordinates, (q,θ,ϕ) , the polarization factors can be written as

$$Q_{\lambda_4}(\vec{k}, \vec{q}) = \frac{q^2}{\sqrt{2}} \sin^2(\theta) \times \begin{cases} \cos(2\phi) & \lambda_4 = + \\ \sin(2\phi) & \lambda_4 = \times. \end{cases}$$
(D7)

Because of the polarization factors, the integral in Eq. (D5) does not vanish only when the connected trispectrum has a nontrivial dependence on the azimuthal angles of \vec{q}_1 and \vec{q}_2 . In the next section, we will show the connected trispectrum in our model does not depend on these angles. This is why the known result, Eq. (16), can be used on our model as if it was Gaussian.

2. The four-point correlation function

We use the same method shown in Appendix B 3 above for the two point correlation, and write an expression analogous to Eq. (B26) for the 4-point correlation, assuming at most a single bubble (which is the leading contribution when expanding in small Γ/V),

$$\langle \delta t_{\vec{x}_{1}} \delta t_{\vec{x}_{2}} \delta t_{\vec{x}_{3}} \delta t_{\vec{x}_{4}} \rangle |_{\leq 1-\text{bubble}} = E \left(\delta t_{\vec{x}_{1}} \delta t_{\vec{x}_{2}} \delta t_{\vec{x}_{3}} \delta t_{\vec{x}_{4}} \Big|_{\text{all pts before } t_{s}}^{\text{bubble with}} \right) P \begin{pmatrix} \text{bubble with all pts before } t_{s} \end{pmatrix}$$

$$+ \sum E \left(\delta t_{\vec{x}_{1}} \delta t_{\vec{x}_{2}} \delta t_{\vec{x}_{3}} \delta t_{\vec{x}_{4}} \Big|_{\text{3 pts before } t_{s}}^{\text{bubble with only}} \right) P \begin{pmatrix} \text{bubble with only} \\ \text{3 pts before } t_{s} \end{pmatrix}$$

$$+ \sum E \left(\delta t_{\vec{x}_{1}} \delta t_{\vec{x}_{2}} \delta t_{\vec{x}_{3}} \delta t_{\vec{x}_{4}} \Big|_{\text{2 pts before } t_{s}}^{\text{bubble with only}} \right) P \begin{pmatrix} \text{bubble with only} \\ \text{2 pts before } t_{s} \end{pmatrix}$$

$$+ \sum E \left(\delta t_{\vec{x}_{1}} \delta t_{\vec{x}_{2}} \delta t_{\vec{x}_{3}} \delta t_{\vec{x}_{4}} \Big|_{\text{3 pts before } t_{s}}^{\text{5 bubble with only}} \right) P \begin{pmatrix} \text{bubble with only} \\ \text{1 pts before } t_{s} \end{pmatrix}$$

$$+ E \left(\delta t_{\vec{x}_{1}} \delta t_{\vec{x}_{2}} \delta t_{\vec{x}_{3}} \delta t_{\vec{x}_{4}} \Big|_{\text{bubble before } t_{s}}^{\text{5 bubble with only}} \right) P \begin{pmatrix} \text{bubble with only} \\ \text{1 pts before } t_{s} \end{pmatrix}$$

$$+ E \left(\delta t_{\vec{x}_{1}} \delta t_{\vec{x}_{2}} \delta t_{\vec{x}_{3}} \delta t_{\vec{x}_{4}} \Big|_{\text{before } t_{s}}^{\text{5 bubble with only}} \right) P \begin{pmatrix} \text{no bubble} \\ \text{before } t_{s} \end{pmatrix}, \tag{D8}$$

where t_s is now defined to be the moment after which no pair of two points is contained in a common Hubble sphere. The sums are over all possible choices of different points to be included in the bubble. As before, in the $\Gamma/V \to 0$ limit the first term is linear in Γ/V , while the others are

of order $(\Gamma/V)^2$ and above. This is because the probability of forming a single bubble is linear in Γ/V , and the expectation values that multiply them have a factor of Γ/V for every $\delta t_{\vec{x}}$ that does not tunnel before t_s .

The first term is given by an expression very similar to Eq. (B30),

$$\int_{0}^{t_{s}} \left(t - \langle t_{\vec{x}} \rangle \right)^{4} \frac{\Gamma}{V} V_{\text{overlap}}(t) dt, \tag{D9}$$

⁵Eq. (D5) has a different coefficient compared to Equation (2.29) in [60] because here we use the dimensionless spectrum.

but this time V_{overlap} is the overlap volume between four Hubble spheres:

$$V_{\text{overlap}}(t) = a^{3}(t) \int_{r_{\mathcal{H}}} d^{3}y_{1} \int_{r_{\mathcal{H}}} d^{3}y_{2} \int_{r_{\mathcal{H}}} d^{3}y_{3} \int_{r_{\mathcal{H}}} d^{3}y_{4}$$

$$\times \delta(\vec{y}_{1} - \vec{y}_{2} + \vec{r}_{2}) \delta(\vec{y}_{1} - \vec{y}_{3} + \vec{r}_{3})$$

$$\times \delta(\vec{y}_{1} - \vec{y}_{4} + \vec{r}_{4})$$
(D10)

where $\vec{r}_i = \vec{x}_i - \vec{x}_1$ are the three independent separations between the \vec{x} 's. In a very similar manner to the above, we Fourier transform the volume to get the contribution to the trispectrum, analogous to Eq. (B32). Omitting numerical coefficients, the result is

$$\mathcal{T}(\vec{k}_{1}, \vec{k}_{2}, \vec{k}_{3}, \vec{k}_{4}) \propto \int_{0}^{\infty} dt (t - \langle t_{\vec{x}} \rangle)^{4} a^{3}(t) \int_{r_{\mathcal{H}}} d^{3} y_{1} e^{i\vec{k}_{1} \cdot \vec{y}_{1}}$$

$$\times \int_{r_{\mathcal{H}}} d^{3} y_{2} e^{i\vec{k}_{2} \cdot \vec{y}_{2}} \int_{r_{\mathcal{H}}} d^{3} y_{3} e^{i\vec{k}_{3} \cdot \vec{y}_{3}}$$

$$\times \int_{r_{\mathcal{H}}} d^{3} y_{4} e^{i\vec{k}_{4} \cdot \vec{y}_{4}}.$$
(D11)

This expression depends only on the magnitudes of the \vec{k} 's, not their directions: $\mathcal{T}(\vec{k}_1, \vec{k}_2, \vec{k}_3, \vec{k}_4) = \mathcal{T}(k_1, k_2, k_3, k_4)$. As mentioned above, this trispectrum gives zero when plugged into Eq. (D5), because of the integral over the azimuthal angle in the polarization factors. This result has a physical interpretation: the leading contribution we have calculated corresponds to the inhomogeneity created by the presence of a single spherical bubble. A spherically symmetric inhomogeneity cannot emit gravitational waves. Contributions to the tunneling due to the formation of

nonspherical bubbles may change this conclusion and consequently strengthen the predicted signal. The study of such effects goes beyond the scope of this paper and is left for future work.

Since the leading term of order Γ/V in Eq. (D8) does not contribute, we have to calculate the $(\Gamma/V)^2$ terms. In Eq. (D8), only the second term is of that order. However, taking the $(\Gamma/V)^2$ order means we have to add terms with the probabilities that two bubbles formed before t_s , which were not present in Eq. (D8). Since we are only interested in terms of order $(\Gamma/V)^2$, the two bubbles have to cover all four points. We split this scenario into three cases:

- (1) One of the bubbles includes all 4 points.
- (2) One bubble includes a single point, and the other bubble includes the remaining the three points.
- (3) Each bubble contains two points.

We neglect the chance of two bubbles forming with a distance smaller than the Hubble radius, H^{-1} , which means the three cases above are distinct. This is justified since the mean distance between bubbles is of order $(\Gamma/V)^{-1/4} \gg H^{-1}$ for an incomplete PT.

The first case has the same symmetry as in the single-bubble calculation above, and therefore gravitational waves are not produced. In the second case, after adding the second term from Eq. (D8), one of the points is independent of the other three, and since $\langle \delta t_{\vec{x}} \rangle = 0$, the contribution to the correlation function is zero. We are therefore only left with the last case, where each of the two bubbles contains two points. The corresponding contribution to the four-point correlation function is then given by a sum over the three possible ways of distributing the four points into two bubbles,

$$\begin{split} \langle \delta t_{\vec{x}_1} \delta t_{\vec{x}_2} \delta t_{\vec{x}_3} \delta t_{\vec{x}_4} \rangle &= \left(\frac{\Gamma}{V} \right)^2 \int_0^{t_{\rm s}} (t - \langle t_{\vec{x}} \rangle)^2 V_{1,2}(t) dt \int_0^{t_{\rm s}} (t - \langle t_{\vec{x}} \rangle)^2 V_{3,4}(t) dt \\ &+ \left(\frac{\Gamma}{V} \right)^2 \int_0^{t_{\rm s}} (t - \langle t_{\vec{x}} \rangle)^2 V_{2,3}(t) dt \int_0^{t_{\rm s}} (t - \langle t_{\vec{x}} \rangle)^2 V_{1,4}(t) dt \\ &+ \left(\frac{\Gamma}{V} \right)^2 \int_0^{t_{\rm s}} (t - \langle t_{\vec{x}} \rangle)^2 V_{1,3}(t) dt \int_0^{t_{\rm s}} (t - \langle t_{\vec{x}} \rangle)^2 V_{2,4}(t) dt \end{split} \tag{D12}$$

where $V_{i,j}$ is the overlap physical volume of two Hubble spheres centered around \vec{x}_i and \vec{x}_j . Each term is in fact a product of two 2-point correlation functions as given by Eq. (B30), so the above correlation satisfies Eq. (D2). This is the promised result: the leading nonvanishing contribution has only a disconnected component, so we can use Eq. (16) safely.

- [1] B. P. Abbott *et al.* (LIGO Scientific and Virgo Collaborations), Phys. Rev. Lett. **116**, 061102 (2016).
- [2] B. P. Abbott *et al.* (KAGRA, LIGO Scientific, and Virgo Collaborations), Living Rev. Relativity **21**, 3 (2018).
- [3] P. Amaro-Seoane, H. Audley, S. Babak, J. Baker, E. Barausse, P. Bender, E. Berti, P. Binetruy, M. Born, D. Bortoluzzi *et al.*, arXiv:1702.00786.
- [4] J. Luo *et al.* (TianQin Collaboration), Classical Quantum Gravity **33**, 035010 (2016).
- [5] J. Crowder and N. J. Cornish, Phys. Rev. D 72, 083005 (2005).
- [6] G. M. Harry, P. Fritschel, D. A. Shaddock, W. Folkner, and E. S. Phinney, Classical Quantum Gravity 23, 4887 (2006); 23, 7361(E) (2006).
- [7] V. Corbin and N. J. Cornish, Classical Quantum Gravity 23, 2435 (2006).
- [8] M. Kramer and D. J. Champion, Classical Quantum Gravity 30, 224009 (2013).
- [9] G. Hobbs, A. Archibald, Z. Arzoumanian, D. Backer, M. Bailes, N. D. R. Bhat, M. Burgay, S. Burke-Spolaor, D. Champion, I. Cognard *et al.*, Classical Quantum Gravity 27, 084013 (2010).
- [10] G. Janssen et al., Proc. Sci. AASKA14 (2015) 037.
- [11] M. Punturo *et al.*, Classical Quantum Gravity **27**, 194002 (2010).
- [12] D. Reitze et al., Bull. Am. Astron. Soc. 51, 035 (2019).
- [13] Z. Arzoumanian *et al.* (NANOGrav Collaboration), Astrophys. J. Lett. **905**, L34 (2020).
- [14] A. H. Guth, Phys. Rev. D 23, 347 (1981).
- [15] A. D. Linde, Phys. Lett. 108B, 389 (1982).
- [16] Y. Akrami *et al.* (Planck Collaboration), Astron. Astrophys. 641, A10 (2020).
- [17] P. A. R. Ade *et al.* (BICEP2, Keck Array Collaborations), Phys. Rev. Lett. **121**, 221301 (2018).
- [18] E. Komatsu *et al.* (WMAP Collaboration), Astrophys. J. Suppl. Ser. **180**, 330 (2009).
- [19] B. Carr, K. Kohri, Y. Sendouda, and J. Yokoyama, Rep. Prog. Phys. 84, 116902 (2021).
- [20] D. J. Fixsen, E. S. Cheng, J. M. Gales, J. C. Mather, R. A. Shafer, and E. L. Wright, Astrophys. J. **473**, 576 (1996).
- [21] D. Baumann, Physics of the Large and the Small (World Scientific, Singapore, 2011), 10.1142/9789814327183_ 0010
- [22] H. Jiang, T. Liu, S. Sun, and Y. Wang, Phys. Lett. B 765, 339 (2017).
- [23] H. An, K.-F. Lyu, L.-T. Wang, and S. Zhou, Chin. Phys. C **46**, 101001 (2022).
- [24] Y.-T. Wang, Y. Cai, and Y.-S. Piao, Phys. Lett. B **789**, 191 (2019).
- [25] H. An, K.-F. Lyu, L.-T. Wang, and S. Zhou, J. High Energy Phys. 06 (2022) 050.
- [26] A. Kosowsky and M. S. Turner, Phys. Rev. D 47, 4372 (1993).
- [27] A. Kosowsky, M. S. Turner, and R. Watkins, Phys. Rev. D 45, 4514 (1992).
- [28] M. Kamionkowski, A. Kosowsky, and M. S. Turner, Phys. Rev. D 49, 2837 (1994).

- [29] S. J. Huber and T. Konstandin, J. Cosmol. Astropart. Phys. 09 (2008) 022.
- [30] C. Caprini, R. Durrer, and G. Servant, Phys. Rev. D 77, 124015 (2008).
- [31] C. Caprini et al., J. Cosmol. Astropart. Phys. 04 (2016) 001.
- [32] C. Caprini et al., J. Cosmol. Astropart. Phys. 03 (2020) 024.
- [33] M. Hindmarsh, S. J. Huber, K. Rummukainen, and D. J. Weir, Phys. Rev. Lett. 112, 041301 (2014).
- [34] J. T. Giblin and J. B. Mertens, Phys. Rev. D **90**, 023532 (2014).
- [35] M. Hindmarsh, S. J. Huber, K. Rummukainen, and D. J. Weir, Phys. Rev. D 92, 123009 (2015).
- [36] T. Kahniashvili, A. Kosowsky, G. Gogoberidze, and Y. Maravin, Phys. Rev. D 78, 043003 (2008).
- [37] T. Kahniashvili, L. Kisslinger, and T. Stevens, Phys. Rev. D 81, 023004 (2010).
- [38] C. Caprini, R. Durrer, and G. Servant, J. Cosmol. Astropart. Phys. 12 (2009) 024.
- [39] K. Schmitz, J. High Energy Phys. 01 (2021) 097.
- [40] M. Lewicki, O. Pujolàs, and V. Vaskonen, Eur. Phys. J. C 81, 857 (2021).
- [41] S. Matarrese, S. Mollerach, and M. Bruni, Phys. Rev. D 58, 043504 (1998).
- [42] S. Mollerach, D. Harari, and S. Matarrese, Phys. Rev. D 69, 063002 (2004).
- [43] K. N. Ananda, C. Clarkson, and D. Wands, Phys. Rev. D 75, 123518 (2007).
- [44] D. Baumann, P. J. Steinhardt, K. Takahashi, and K. Ichiki, Phys. Rev. D 76, 084019 (2007).
- [45] K. Kohri and T. Terada, Phys. Rev. D 97, 123532 (2018).
- [46] J.R. Espinosa, D. Racco, and A. Riotto, J. Cosmol. Astropart. Phys. 09 (2018) 012.
- [47] S. Coleman and F. De Luccia, Phys. Rev. D 21, 3305 (1980).
- [48] S. W. Hawking and I. G. Moss, Adv. Ser. Astrophys. Cosmol. 3, 154 (1987).
- [49] A. H. Guth and E. J. Weinberg, Nucl. Phys. B212, 321 (1983).
- [50] M. S. Turner, E. J. Weinberg, and L. M. Widrow, Phys. Rev. D 46, 2384 (1992).
- [51] A. A. Starobinsky, Lect. Notes Phys. 246, 107 (1986).
- [52] A. D. Linde, Contemp. Concepts Phys. 5, 1 (1990).
- [53] J. Chluba, A. L. Erickcek, and I. Ben-Dayan, Astrophys. J. 758, 76 (2012).
- [54] P. E. Dewdney, P. J. Hall, R. T. Schilizzi, and T. J. L. W. Lazio, Proc. IEEE **97**, 1482 (2009).
- [55] B. S. Sathyaprakash and B. F. Schutz, Living Rev. Relativity **12**, 2 (2009).
- [56] C. J. Moore, R. H. Cole, and C. P. L. Berry, Classical Quantum Gravity **32**, 015014 (2015).
- [57] W. Ratzinger and P. Schwaller, SciPost Phys. 10, 047 (2021).
- [58] G. F. Giudice, M. McCullough, and T. You, J. High Energy Phys. 10 (2021) 093.
- [59] D. Curtin, P. Meade, and H. Ramani, Eur. Phys. J. C 78, 787 (2018).
- [60] P. Adshead, K. D. Lozanov, and Z. J. Weiner, J. Cosmol. Astropart. Phys. 10 (2021) 080.